HHS Public Access

Author manuscript

Neurobiol Dis. Author manuscript; available in PMC 2016 March 01.

Published in final edited form as:

Neurobiol Dis. 2015 March ; 75: 142–150. doi:10.1016/j.nbd.2014.12.029.

PTEN deletion from adult-generated dentate granule cells disrupts granule cell mossy fiber axon structure

Candi L. LaSarge[1], **Victor R Santos**[1,2], and **Steve C. Danzer**[1,3]

[1]Department of Anesthesia, Cincinnati Children's Hospital Medical Center, Cincinnati, OH, 45229

[2]Department of Physiology, Ribeirão Preto Medical School, Ribeirão Preto-SP, Brazil

[3]Departments of Anesthesia and Pediatrics, University of Cincinnati, Cincinnati, OH, 45267

Abstract

Dysregulation of the mTOR-signaling pathway is implicated in the development of temporal lobe epilepsy. In mice, deletion of PTEN from hippocampal dentate granule cells leads to mTOR hyperactivation and promotes the rapid onset of spontaneous seizures. The mechanism by which these abnormal cells initiate epileptogenesis, however, is unclear. PTEN-knockout granule cells develop abnormally, exhibiting morphological features indicative of increased excitatory input. If these cells are directly responsible for seizure genesis, it follows that they should also possess increased output. To test this prediction, dentate granule cell axon morphology was quantified in control and PTEN-knockout mice. Unexpectedly, PTEN deletion increased giant mossy fiber bouton spacing along the axon length, suggesting reduced innervation of CA3. Increased width of the mossy fiber axon pathway in stratum lucidum, however, which likely reflects an unusual increase in mossy fiber axon collateralization in this region, offset the reduction in boutons per axon length. These morphological changes predicts a net increase in granule cell >> CA3 innervation. Increased diameter of axons from PTEN-knockout cells would further enhance granule cell >> CA3 communication. Altogether, these findings suggest that amplified information flow through the hippocampal circuit contributes to seizure occurrence in the PTEN-knockout mouse model of temporal lobe epilepsy.

Keywords

epilepsy; PTEN; mTOR; dentate granule cells; mossy fibers; hippocampus

Corresponding author: (Laboratory of Origin) Dr. Steve C. Danzer 3333 Burnet Avenue, ML 2001 Cincinnati, Ohio 45229-3039 (513) 636-4526 (phone) (513) 636-7337 (fax) steve.danzer@cchmc.org.

Introduction

Dentate granule cells are a major component of the classic hippocampal trisynaptic circuit, receiving information from the entorhinal cortex and passing it through long, unmylenated mossy fiber axons onto the apical dendrites of the CA3 pyramidal cells. In a normal brain, the dentate granule cells are hypothesized to block the throughput of excess excitation into the hippocampus, acting as a gate or filter (Hsu, 2007). It is hypothesized that a breakdown of this filtering occurs during temporal lobe epilepsy (TLE), resulting in excessive signaling to CA3. Changes in granule cell structure and connectivity coincide with the onset of spontaneous seizures and might facilitate this breakdown (Dudek and Sutula, 2007, Ben-Ari and Dudek, 2010, Cameron et al., 2011, Santos et al., 2011, Murphy et al., 2012, Parent and Kron, 2012, Scharfman and Pierce, 2012, Hester and Danzer, 2013, Singh et al., 2013, Hester and Danzer, 2014).

Mossy fiber axons have three types of presynaptic terminals: giant mossy fiber boutons, filopodial extensions of these boutons and *en passant* terminals. Mossy fiber boutons synapse with elaborate clusters of spines - thorny excrescences - located on the basal and apical dendrites of the CA3 pyramidal cells. Each mossy fiber axon gives rise to approximately 15 giant boutons, and individual CA3 pyramidal cells can receive input from up to 50 granule cells (Amaral et al., 1990). Filopodial extensions and *en passant* terminals, on the other hand, form synapses with the GABAergic interneurons (Frotscher, 1989, Acsády et al., 1998, Seress et al., 2001). The filopodial and *en passant* terminals are responsible for another 40 to 50 synapses per mossy fiber axon, allowing for feed-forward inhibition to regulate CA3 network excitability (Acsády et al., 1998). Structural plasticity of the mossy fiber axons and boutons has been noted in animal models of TLE. In fact, epileptogenesis has been associated with increased bouton density, increased number of release sites, increased active zone length and changes in the distribution of thorny excrescences of the CA3 pyramidal cells (Goussakov et al., 2000, Danzer et al., 2010, McAuliffe et al., 2011, Upreti et al., 2012). Enhanced connectivity between granule cells and CA3 pyramidal cells, therefore, may promote epileptogenesis in traditional models of TLE.

Recently, our lab described a novel transgenic mouse model of TLE, in which the mammalian target of rapamycin (mTOR) pathway inhibitor phosphatase and tensin homologue (PTEN) could be selectively deleted from adult born granule cells (Pun et al., 2012). These mice developed spontaneous seizures beginning 4-6 weeks following gene deletion. Enhanced mTOR signaling among granule cells is a common feature of a variety of TLE models (Brewster et al., 2013, Wong, 2013, Lasarge and Danzer, 2014), so the observation that PTEN deletion is sufficient to cause epilepsy suggests enhanced mTOR signaling may play a critical role in epileptogenesis. The mechanisms by which increased mTOR signaling in dentate granule cells (DGCs) might promote epilepsy, however, are unclear. One possibility is that increased mTOR activation in DGCs induces structural changes in their mossy fiber axons, supporting increased signaling to CA3. Increased DGC >> CA3 connectivity would facilitate seizure spread through the hippocampus. To explore this possibility, mossy fiber axon structure was examined in GFP-expressing PTEN-knockout (KO) and control mice.

Material and methods

Animals

All procedures were approved by the CCHMC Animal Board (IACUC) and followed NIH guidelines. Three transgenic lines were used for these studies: Gli1-CreER^{T2} mice, CAG-CAT-enhanced green fluorescent protein (GFP) reporter mice, and Pten^{tm1Hwu}/J mice (Jackson Laboratory). Gli1-CreER^{T2} expressing mice have a cDNA encoding CreER^{T2} inserted into the 5'UTR of the first coding exon of the Gli1 locus (Ahn and Joyner, 2004, Ahn and Joyner, 2005). GFP reporter mice possess a CAG-CAT-EGFP reporter construct driven by a CMV-ß actin promoter regulated by loxP flanked CAT gene (Nakamura et al., 2006). The Gli1-CreER^{T2} and GFP mice were crossed with Pten^{tm1Hwu}/J mice, in which loxP sites were placed on either side of exon 5 of the PTEN gene (PTEN "floxed" mice). Study animals were generated by crossing Gli1-CreER^{T2} hemizygous, PTEN$^{flox/wt}$ male mice with GFP reporter heterozygous (+/−) or homozygous (+/+), PTEN$^{flox/wt}$ mice. Animals used in this study were hemizygous for the Gli1-CreER^{T2} and GFP reporter transgenes. All mice were maintained on a C57BL/6 background, and whenever possible, littermate controls were used. All mice used for studies (except one control) were injected with tamoxifen (250 mg/kg dissolved in corn oil) subcutaneously on postnatal day (P) 14. At this age, the only Gli1-expressing neural progenitor cells still active in the CNS are subgranular zone progenitors, which produce DGCs, and subventricular zone progenitors that produce olfactory neurons (Ming and Song, 2005). Therefore, recombination is restricted to a subset of neurons among these populations.

Mice used for morphological analysis included the following genotypes: Gli1-CreER^{T2}::PTEN$^{flox/flox}$::GFP reporter [GFP^{+}KO; n=10; 7 male, 3 female] and Gli1-CreER^{T2}::PTEN$^{flox/flox}$ [KO; n=6 males]. Controls consisted of mice with Gli1-CreER^{T2}::PTEN$^{wt/wt}$::GFP reporter [GFP^{+}Cre control, n=9; 5 male, 4 female] and Gli1-CreER^{T2} negative, PTEN$^{flox/flox}$ genotypes [flox control, n=6 males]. Mice were separated into two age groups. A subset of mice were perfused at 6 weeks of age [early adult; 3 GFP^{+}KO and 3 GFP^{+}Cre control] and the remaining mice were aged between 2.25 and 7 months (mature adult; controls, mean age = 4.9 ± 0.82 months; KOs, mean age = 3.79 ± 0.40 months). EEG and dendrite morphology data on a subset of these animals has been presented previously (Pun et al., 2012). An additional 10 male mice (6 KO, 3 flox control and 1 cre control) aged 3 to 9 months were used to make acute slices for single-cell biocytin injections. Finally, one Gli1-CreER^{T2}::PTEN$^{flox/flox}$ was not treated with tamoxifen and served as a cre/flox control for biocytin injection. All other controls received tamoxifen.

In a previous study, animal sex was found to have no effect on several morphological measures of PTEN-KO cell morphology (Pun et al., 2012). In the present study, sex had no effect on any of the axon parameters examined, including boutons per axon ($p=0.442$), axon thickness ($p=0.257$), and volume of mossy fiber boutons ($p=0.105$). Therefore, male and female animals were pooled for statistical analyses.

Immunohistochemistry

Animals for morphological analysis were overdosed with pentobarbital (100 mg/kg) and perfused with phosphate-buffered saline (PBS) +1U/ml heparin, followed by 2.5% paraformaldehyde and 4% sucrose in PBS (pH 7.4). Brains were post-fixed overnight, cryoprotected and sectioned sagittally on a cryostat at 40 μm. Sections were mounted to gelatin-coated slides and stored at −80°C until use. Triple immunostaining of brain sections was conducted using chicken anti-GFP (1:3000, Abcam, Cambridge, UK), rabbit anti-PTEN (1:250, Cell Signaling Technology, Inc., Danvers, MA) and mouse anti-NeuN (1:400, Millipore, Temecula, CA) antibodies to confirm PTEN deletion and to assess mossy fiber axon and bouton morphology. Adjacent sections were immunostained with anti-GFP and anti-ZnT-3 (1:500, Synaptic Systems, Gottingen, Germany) to assess the width of stratum lucidum and mossy fiber sprouting into the dentate inner molecular layer. Alexafluor 488 goat anti-chicken, Alexafluor 594 goat anti-rabbit and Alexafluor 647 goat anti-mouse secondary antibodies were used for all immunostaining (all at 1:750, Invitrogen, Grand Island, NY). For each animal, between two and four brain sections corresponding to medial-lateral coordinates 1.3 – 1.7 mm were examined (Paxinos and Franklin, 2001). GFP images were collected with a Nikon A1+ inverted microscope equipped with 10X (NA 0.45) and 100X oil (NA 1.49) objectives (Nikon Instruments Inc., Melville, NY). GFP and ZnT-3 colabeled images were collected using a Leica SP5 confocal system equipped with a 63X oil (NA 1.4) objective (Leica Microsystems Inc., Buffalo Grove, IL). All analyses and counts were conducted by an investigator unaware of treatment group.

Anatomical measurements: Stratum lucidum

Mossy fiber axons of GFP-expressing dentate granule cells from PTEN KO and control mice were imaged in stratum lucidum of CA3b, as defined by Lorente de Nó, (1934). More specifically, image stacks were collected from the middle of the region of CA3 that lies between the tips of dentate gyrus blades and the fimbria (Ishizuka et al., 1995). Regions were selected using a 10x objective, and images were collected using a 100x oil objective (image size 0.12 μm/px, 1024 × 1024) with a 0.1μm step through the z-axis. The same image stack for each animal was used for analyses of axon thickness, boutons per μm of axon length and giant bouton volume. A single two-channel confocal image of the same region of stratum lucidum was collected of GFP-expressing mossy fiber axons and ZnT-3 labeling using a 63X objective (image size 0.24 μm/px, 1024x1024 format) for measurement of stratum lucidum width.

Mossy fiber axon cross-sectional area and boutons per mossy fiber axon length

Image stacks were imported into Neurolucida software (MBF Bioscience, Williston, VT) for analysis. Mossy fiber axons were traced and attached boutons marked. Average length traced from GFP^{+}Cre control mice was 1056 ± 207 μm, while 1874 ± 375 μm of axon were traced from GFP+KO mice. The number of attached boutons was divided by the μm of axon length traced to calculate boutons per mossy fiber length. To calculate the diameter of the mossy fiber axons from each animal, 100-200 μm of axon for each animal was randomly selected and traced using lines with graded thickness that matched the axonal thickness.

Four to seven traced axonal segments were used to determine average axon diameter for each animal.

Mossy fiber bouton volumetric measurement

Image stacks from mature adult mice were imported into Imaris (v. 7.6, Bitplane AG, Zurich, Switzerland) for 3D visualization and reconstruction. Surface models of 3D image stacks (Surface grain 0.4, threshold >480, seed point = 2.5; split surface) were created. All boutons cut by the boundaries of the scan were excluded, so that only whole boutons were modeled. Volumes less than 6 μm^3 were filtered out to account for the spherical equivalent to previously-reported cross-sectional area minima of 4 μm^2, which has been used to distinguish giant mossy fiber boutons from smaller *en passant* terminals, mitochondria accumulations or tissue artifacts (Claiborne et al., 1986, Acsády et al., 1998, Danzer et al., 2010). All statistical measurements were exported to Excel (Microsoft Office, WA) and average volumes were calculated for each animal.

Anatomical measurements: Dentate gyrus

Immunostaining of PTEN and NeuN in the dentate gyrus was imaged with a 0.5 μm step through the z-axis (63X, image size 0.24 μm/px, 1024×1024 format) to estimate the percentage of KO cells (PTEN negative / NeuN expressing cells) in each mouse. Image stacks were imported into Neurolucida software and a modification of the optical dissector method was used to quantify the number of KO cells (Howell et al., 2002, Pun et al., 2012). Mossy fiber sprouting was scored from two-channel confocal optical sections of the dentate inner molecular layer (63X, image size 0.12 μm/px, 2024×2024 format) collected from the midpoint of the upper blade of the dentate. Optical sections were captured 2-3 μm below the tissue surface to ensure equivalent antibody penetration, staining and image quality. Mossy fiber sprouting was scored by determining the percentage of the total inner molecular layer area occupied by ZnT-3 immunoreactive puncta using automatic object detection (Neurolucida). Sensitivity for automatic detection was set to capture all puncta more than 2X background and larger than 0.5 μm^2. All automated counts were reviewed manually to insure accuracy.

Axon tracing of biocytin-filled cells

Biocytin was injected into dentate granule cells in acute slices made from control (n=5) and PTEN KO mice (n=6). In order to prepare hippocampal slices, mice were anesthetized with an injection of pentobarbital (100 mg/kg) and perfused intracardially with ice-cold modified ACSF of the following composition (mM): NaCl, 92; KCl, 2.5; NaH_2PO_4, 1.25; $NaHCO_3$, 30; $MgSO_4$, 10; $CaCl_2$, 0.5; Na pyruvate, 3; thiourea, 2; Na ascorbate, 5; glucose, 25; HEPES, 20. The brain was removed and 350 μm transverse slices (as described by Jones and Heinemann, 1988) were prepared on a tissue slicer (Campden/Lafayette Instrument, IN). Individual slices were transferred to an N-methylD-glutamine (NMDG)-based medium (similar to the modified ACSF with the exception that the NaCl was substituted with NMDG, 92mM) and equilibrated for 60 minutes. The modified ASCF and NMDG solutions used are as described by Ting and colleagues (2014). After 60 minutes, the slices were transferred into recording ACSF for another 60 minutes. ACSF was of the following

composition and concentration (mM): NaCl, 124; KCl, 3.5; $MgSO_4$, 2; $CaCl_2$, 2; NaH_2PO_4, 1.25; glucose, 10; $NaHCO_3$, 26. Individual slices were placed in the stage chamber of an upright microscope (Nikon, Eclipse FNI) equipped with a 10X bright field and a 40X DIC objective. Slices were continuously perfused with ACSF. Cells were filled with biocytin using blunt-tipped patch electrodes filled with K gluconate, 135; KCl, 5; NaCl, 5; EGTA, 5; HEPES, 10, $MgCl_2$, 2; glucose, 10 supplemented with 2mM of ATP and 200 μM of GTP; and 0.2% biocytin. All extracellular solutions used had a pH between 7.2 and 7.3, osmolarity of 290-300 mOs (adjusted by addition of sucrose) and were continuously aerated with a mixture of 5% CO_2 and 95% O_2. All experiments were carried out at room temperature. After biocytin filling, slices were put into fixative and left overnight (2.5% formaldehyde and 4% sucrose in PBS). The next day, slices were permeablized in 0.5% Igepal in PBS for one hour and incubated in Alexa Fluor 594-streptavidin (1:500; Invitrogen, Grand Island, NY) for four hours at 4°C or two hours at room temperature with continuous shaking. Labeled cells were tile-scanned on a Nikon A1+ inverted confocal microscope equipped with 10X (NA 0.45) and 40X water (NA 1.15) objectives. The dentate, dentate hilus and CA3 stratum lucidum were imaged to capture the axon (0.31 μm/px, 1024x1024 format, z-step = 0.5 μm). Image stacks were imported into Neurolucida software for cell body and mossy fiber axon tracing. Sholl analyses, with sphere radii set at 250 μm, were also conducted.

It was not possible to conduct PTEN immunohistochemistry in biocytin filled slices due to poor antibody penetration through the thick tissue, so PTEN KO cells were distinguished from “wildtype” PTEN-expressing cells in the same tissue by their larger somatic size (Luikart et al., 2011, Amiri et al., 2012, Pun et al., 2012, Sperow et al., 2012). Thus, all cells from PTEN KO mice were classified as PTEN KO cells since their cross-sectional areas were at least two standard deviations greater than the mean of dentate granule cells from control mice (control cell soma area, 116.27 ± 17.59 μm^2; mean±SD). All control cells analyzed were from control mice.

Statistics and data analysis

For all analyses, statistical significance was determined using Sigma Plot software (version 12.5, Systat Software, Inc., San Jose, CA). Specific tests were used as noted in the results. Data are presented as means ± standard error or median and range.

Figure preparation

All images are either single confocal optical sections or confocal maximum projections exported as TIFF files and imported into Adobe Photoshop (version 12.0.1, Adobe Systems, San Jose, CA). Images were adjusted using Nikon Elements median filter (radius=3) or Leica Application Suite with a morphological erosion filter (radius=3; iterations=1) to reduce background artifact. Brightness and contrast of digital images were adjusted to optimize cellular detail. Identical adjustments were made to all images meant for comparison.

Results

PTEN deletion among a subset of granule cells

In control and PTEN KO mice, GFP-expressing dentate granule cells were located close to the hilar border, as predicted for post-natally generated neurons; although a subset of cells were located ectopically in the hilus in PTEN KO mice. GFP expression was detected throughout the cell body, dendrites, and mossy fiber axons (Figure 1). Expression was robust, allowing for the morphological characterization of mossy fiber axons and terminals at high resolution (Figure 1G, 1H). PTEN deletion was confirmed by triple immunostaining for GFP, PTEN, and NeuN in brain sections. GFP-expressing cells in the control animals were co-labeled with PTEN antibodies; whereas PTEN antibody labeling was absent from GFP-expressing cells in PTEN KO animals (Figure 1C, 1D). Characterization of PTEN KO granule cells revealed abnormal cellular morphologies, including hypertrophied somas, hilar ectopic cells, mossy fiber sprouting, and basal dendrites (Kwon et al., 2001, Amiri et al., 2012, Pun et al., 2012). The percentage of granule cells that lacked PTEN ranged from 3.1 to 26.5 percent in KO animals.

PTEN-knockout cells exhibit giant mossy fiber boutons at greater intervals along their axons

Dentate granule cells synapse onto the proximal apical and basal dendrites of CA3 pyramidal cells via giant mossy fiber boutons. Changes in bouton number or size, therefore, predict alterations in output to CA3. To determine whether PTEN deletion alters mossy fiber structure, mossy fiber axons were reconstructed from confocal images of mature adult control and PTEN KO animals (Figure 2). Approximately 1000-2000 μm of mossy fiber axon per animal was reconstructed. Surprisingly, PTEN KO mice had fewer boutons per 100 μm axon length compared to the control mice (KO, 0.93 ± 0.13; control, 1.4 ± 0.12, t= 2.406, p=0.042, t-test; Figure 2E). Axons from control animals had a giant bouton roughly every 71.4 μm, while KO mossy fiber boutons were spaced at 106.4 μm intervals. Paradoxically, these changes predict a less excitable hippocampal circuit, rather than the increased excitability evident in these animals (e.g. the occurrence of spontaneous seizures).

PTEN-knockout cells exhibit normal mossy fiber bouton volume

Individual mossy fiber giant boutons possess numerous synaptic release sites, with larger boutons possessing more sites (Pierce and Milner, 2001). A reduction in bouton density could be offset by an increase in the number of release sites, which can be assessed indirectly by examining bouton volume. To determine whether PTEN KO cells exhibited altered mossy fiber bouton volume, Imaris image analysis software was used to three-dimensionally reconstruct the boutons from high resolution confocal images (Figure 3). Mossy fiber bouton volume did not differ between control (27.7 ± 3.1 μm^3; n=5 mice, 22-74 boutons measured/mouse) and PTEN KO (23.5 ± 2.0 μm^3; n=6 mice, 23-95 boutons measured/mouse) mice (t = −1.175, *n.s.*, p=0.27, t-test). The ranges of bouton volume were also similarly distributed in all animals. Specifically, mice exhibited a positive skew in their bouton size distribution, with large numbers of small boutons and small numbers of large boutons [Control skew range: (0.81-1.36); PTEN KO skew range: (0.88-1.47)]. Although the measure is indirect, these results suggest that giant boutons in control and KO mice

possess similar numbers of release sites. Changes in individual bouton strength, therefore, seem unlikely to account for hyperexcitability in the mice.

Mossy Fiber Axon growth

Although measures of bouton density revealed a decrease per length of axon, casual analysis of stratum lucidum seemed to suggest that the number of giant boutons actually increased. Specifically, in KOs, stratum lucidum appeared thicker with more boutons populating the mossy fiber tract. One variable that could account for these seemingly paradoxical observations is excessive mossy fiber axon growth. Bouton density per axon might decrease, but if KO cell axons are longer, then total bouton number could still be greater. Indeed, previous observations of mossy fiber sprouting into the dentate inner molecular layer in these animals (Pun et al., 2012), and confirmed again here for a subset of mature adult animals (Figure 4 C and D), clearly establishes that the axons can grow excessively within the dentate.

To determine whether excessive axon growth might also be occurring in the CA3 region, we first examined stratum lucidum using zinc transporter 3 (ZnT-3) immunolabeling. ZnT-3 protein is abundant in the mossy fiber terminals, and antibodies for the protein robustly label terminals in stratum lucidum of CA3 (Figure 4 E and F), where mossy fibers synapse onto pyramidal cell thorny excrescences. Stratum lucidum width was increased in mature adult PTEN KO mice vs. controls (65.4 ± 4.7 μm vs. 48.8 ± 2.0 μm, respectively; t= 3.121, p=0.005, t-test). The increased stratum lucidum width could simply reflect greater dispersion of fibers and terminals among KO cells, so we also quantified terminal density by determining the percentage of a fixed region of stratum lucidum CA3b that was occupied by ZnT-3 immunoreative puncta (as seen in Figure 4 E and F). This analysis revealed no difference in percentage of stratum lucidum occupied by puncta between PTEN KO and control mice (KO, 14.21 ± 0.84%; control, 13.60 ± 1.38%; t= 0.617, n.s.), indicating that boutons are not more dispersed in these mice. Given similar bouton density in PTEN KO mice, the 34% increase in the width of stratum lucidum would imply a similar increase in the total number of boutons. Overall, these findings suggest that the increased distance between boutons along mossy fiber axons might be more than offset by increased axon growth, preserving or even increasing granule cell - pyramidal cell innervation ratios.

PTEN KO granule cells have abnormal axon growth

GFP labeling of large numbers of cells in GFP^{+}KO mice precludes tracing of individual axons. In order to investigate the possibility that PTEN KO animals have increased mossy fiber axon growth in CA3, therefore, axons of individual dentate granule cells were analyzed. To accomplish this, granule cells from PTEN KO and control mice were filled with biocytin in acute hippocampal slices. All control cells (N=5) exhibited axon branching patterns consistent with previously-published work (for review see Amaral et al., 2007, Blaabjerg and Zimmer, 2007). The axons of these cells collateralized extensively in the dentate hilus, but projected only a single, unbranched fiber into CA3 stratum lucidum (Figure 5A and the cell tracing seen in 5A'). By contrast, 33% of PTEN KO cells (two of six) projected dual axon collaterals into CA3 stratum lucidum (Figure 5B, tracing shown in 5B'). Indeed, these axons continued to branch after entering CA3 stratum lucidum, a feature

also absent from control cells. Additionally, a third cell exhibited a mossy fiber axon that extended through the granule cell layer and into the molecular layer (Figure 5C and 5C'). A Sholl analysis indicated that the percent of the axon that was located within 250 μm of the soma was greater in the control mice (PTEN KO: 54.72 ± 6.67%; Control: 78.56 ± 2.28%; t= 3.12, p=0.01, t-test), while PTEN KO cells exhibited greater axon length in more distal regions of the axonal tree. Total axon length measured was similar in both groups; PTEN KO: 1635.74 μm ± 250.55 and controls: 1769.52 μm ± 209.03. Altogether, single-cell reconstructions revealed that PTEN KO axons have greater axon length in CA3 than controls, can contribute to mossy fiber sprouting in the dentate inner molecular layer, and can exhibit multiple axon branches in CA3 stratum lucidum.

PTEN-knockout cells exhibit increased mossy fiber axon diameter

Another important feature of the mossy fiber axon is its diameter. Mossy fibers are unmyelinated, so changes in axonal diameter could significantly affect conduction velocity and efficiency of information transmission. To determine whether this parameter might be altered, axon diameter was measured over 100-200 μm of axon length for each control and PTEN KO mouse. As illustrated in Figure 2, mossy fiber axon diameter was significantly increased in mature adult PTEN KO mice (0.697 ± 0.057 μm; t= 2.396, p=0.043, t-test; Figure 2F) compared to controls (0.505 ± 0.022 μm). Moreover, the average diameter of the GFP-expressing axons was inversely correlated with the average bouton density (R=0.680, p=0.030, Pearson Correlation; Figure 2G), such that those animals with the thickest axons had the fewest boutons per length of axon. Thicker axons would be predicted to increase conduction efficiency, and could enhance throughput of excitation to CA3 pyramidal cells.

Changes in axon morphology appear within weeks of PTEN deletion

PTEN KO mice develop spontaneous seizures. Morphological changes in these animals, therefore, likely reflect a combination of direct and indirect effects. To explore whether direct or indirect effects account for the changes described in the present study, early adult PTEN KO and control mice were examined four weeks after gene deletion (when mice are six weeks old). At this time point, GFP-labeled granule cells begin to display typical mature cell morphology (for review see Zhao et al., 2008) and seizures are likely to be infrequent or absent. Similar to older animals, axonal hypertrophy was evident in early adult PTEN KO mice (Figure 6; PTEN KO axon diameter = 0.582 ± 0.010 μm; control = 0.423 ± 0.030 μm; t= 4.984, p=0.008, t-test). Moreover, it appears that the increase in bouton spacing may coincide with axon development. Early adult PTEN KO mice showed a trend towards fewer boutons per 100 μm axon length compared to age-matched controls (KO, 0.72 ± 0.07; control, 1.3 ± 0.28, t= 0.616, p=0.098, t-test). As in mature adult mice, the average diameter of the developing GFP-expressing axons was inversely correlated with the average bouton density per axon length (R=0.891, p=0.017, Pearson Correlation). Finally, an examination of ZnT-3 labeling in CA3b revealed an increase in stratum lucidum width in early adult PTEN KO mice compared to controls (PTEN KO: 49.69 ± 0.8 μm; control: 34.08 ± 4.1 μm; t= 3.769, p=0.020, t-test). The rapid appearance of these morphological changes suggests they are a direct, cell-autonomous effect of PTEN deletion rather than a secondary consequence of seizure activity.

Discussion

Mice with PTEN deleted from a subset (>9%) of adult-born dentate granule cells develop spontaneous seizures as early as four weeks after gene deletion (Pun et al., 2012). The mechanism by which PTEN KO cells promote epilepsy, however, remains unclear. It has been previously shown that PTEN KO cells have morphological abnormalities indicative of increased excitatory input, including *de novo* basal dendrites and greater dendritic spine density (Pun et al., 2012). Here, we explored whether PTEN KO cells also exhibit changes indicative of increased output. Dentate granule cells are a key part of the classic hippocampal tri-synaptic circuit, so enhanced output to the next part of this circuit, the CA3 pyramidal cell, could be a key change driving epileptogenesis. Our results support the conclusion that granule cell innervation of CA3 pyramidal cells is enhanced in PTEN KO mice. While the number of giant boutons per mossy fiber axon length was reduced for KO cells, axon length and stratum lucidum width in CA3 were increased. Bouton density in CA3 stratum lucidum was similar in control and KO mice, so the increased stratum lucidum width would support a great number of terminals. Finally, PTEN KO cells had thicker axons, which could further enhance conduction and transmission to CA3. These morphological abnormalities were found as early as four weeks after gene deletion, suggesting they are a direct effect of PTEN loss. Taken together, these finding provide morphological evidence that the granule cell >> CA3 pyramidal cell portion of the hippocampal trisynaptic circuit is strengthened in PTEN KO mice. These changes might contribute to seizure occurrence in this model.

PTEN deletion alters mossy fiber branching and distribution

Several lines of evidence suggest that the axonal derangements produced by PTEN deletion are likely due to mTOR hyperactivation (Kwon et al., 2006, Choi et al., 2008, Faulkner et al., 2008, Zeng et al., 2009, Zhou et al., 2009, Huang et al., 2010, Buckmaster and Lew, 2011, Amiri et al., 2012, Pun et al., 2012). Firstly, findings from other studies strongly implicate the mTOR pathway in regulating granule cell axon growth. For example, PTEN deletion using alternate cre-drivers, and deletion of tuberous sclerosis protein 1 (TSC1) - another negative regulator of mTOR - all produce progressive mossy fiber tract enlargement (Kwon et al., 2006, Zhou et al., 2009, Amiri et al., 2012). Other models with increased mTOR signaling have also shown axonal defects. Knockdown of the protein disrupted in schizophrenia 1 (Disc1), which regulates mTOR signaling via the AKT binding protein KIAA1212 (Kim et al., 2009), caused mistargeting of mossy fibers and growth outside of the stratum lucidum and into CA1 (Faulkner et al., 2008). Similarly, treatment of granule cells *in vitro* with brain-derived neurotrophic factor (an mTOR pathway activator) increased axon branching (Patel and McNamara, 1995). Conversely, administration of the mTOR antagonist rapamycin reduced mossy fiber axon tract thickness and prevented axonal targeting defects like mossy fiber sprouting in both genetic and acquired epilepsy models (Zeng et al., 2009, Zhou et al., 2009, Huang et al., 2010, Buckmaster and Lew, 2011, Pun et al., 2012, Yamawaki et al., 2015). Finally, the rapid appearance of stratum lucidum thickening only four weeks after PTEN deletion (when granule cells are still maturing) suggests that mTOR directly regulates axonal development, rather than producing its many effects secondarily, such as by promoting ictal events.

Bouton structure is conserved in PTEN KO mice

Mossy fiber bouton structure appears to be unaltered in PTEN KO mice. This result is consistent with previous findings that giant boutons in Disc1 knockdown mice were comparable to controls (Faulkner et al., 2008). However, these data are in contrast to pilocarpine-induced epilepsy in rodents, which is associated with increased giant bouton area (Danzer et al., 2010, McAuliffe et al., 2011, Upreti et al., 2012). It seems unlikely, therefore, that changes in bouton size evident in the pilocarpine model are mediated by enhanced mTOR signaling. Spontaneous seizures in the pilocarpine model follow the induction of status epilepticus, while PTEN KO mice form their abnormal network during cell development in lieu of an overt epileptogenic insult. Status epilepticus induces widespread brain injury, including cell death in dentate hilus, CA3 and CA1 pyramidal cell layers and cortex (Shibley and Smith, 2002, Borges et al., 2003, Curia et al., 2008, Danzer et al., 2010). Differences in the severity of the epileptogenic insult may account for the differences in giant bouton regulation between the seizure models.

Increased bouton spacing

The interval between boutons is increased along PTEN KO cells axons. It has previously been hypothesized that mice with fewer mossy fibers in CA3 stratum lucidum experience less competition for available postsynaptic sites (Nek et al., 1993). If competition for postsynaptic sites is a factor in bouton spacing, then the increase in distance between boutons in PTEN KO animals may be a consequence of additional axons in the stratum lucidum. Moreover, it is also possible that increased axon diameter impacts the ability of multiple axons to form synapses on individual dendrites. In fact, in our mice there was a correlation between mossy fiber diameter and the distance between boutons, supporting the idea that increased axon diameter in PTEN KO mice may create a spacing problem. This competition for space could also contribute to the thickening of stratum lucidum, as axons might be forced to target more distal dendritic sites. Notably, Sutula and colleagues (1998) described a pattern of increased axon length and decreased number of giant boutons per axon length in the kainic acid model of epilepsy, providing further correlative evidence of an inverse relationship between the two variables. It is worth noting, however, that the mTOR signaling pathway could also regulate granule cell bouton spacing via cell intrinsic mechanisms. Indeed, a trend towards increased spacing was already evident four weeks after PTEN deletion, implying a possible direct effect. Analysis of PTEN KO animals with very low numbers of mature KO cells, such that fiber number in stratum lucidum is not significantly changed, might provide insight into this question.

Significance for epileptogenesis

Hyperexcitability in the dentate gyrus has been hypothesized to result from a small number of hub cells, defined as neurons with enhanced incoming and outgoing connectivity that could mediate the failure of the dentate gate (Morgan and Soltesz, 2008). The morphological changes described here, combined with previous data examining PTEN KO cell inputs, suggest that these neurons could be acting as hub cells. Previous studies have demonstrated that cells with mTOR hyperactivation have increased excitatory input. PTEN knockdown increases miniature excitatory post-synaptic currents (mEPSCs) and spontaneous post-

synaptic currents in dentate granule cells (Luikart et al., 2011). Haws and colleagues (2014) found similar results with PTEN knockdown in basolateral amygdala, in which mEPSC frequency and amplitude increased. Additionally, hippocampal pyramidal cells with TSC1 deletion exhibited increased mEPSC frequency (Bateup et al., 2011). The present study adds to these findings by presenting anatomical evidence that PTEN KO cells also have enhanced output to CA3. Axonal sprouting and greater bouton numbers would increase CA3 pyramidal cell innervation, while increased axon thickness would support enhanced efficiency and probability of synaptic transmission via these inputs (Rushton, 1951). Mossy fiber axon synapses onto CA3 pyramidal cells are already considered to be one of the most powerful connections in the CNS, previously termed the “detonator” synapses due to their ability to fire the target pyramidal cells (Henze et al., 2002). Increased axon diameter could further enhance this already powerful synapse. Finally, we note that the predicted minimum number of hub cells required to provoke network instability in Morgon and Soltesz’s computation modeling study (5%) is lower than the number of PTEN KO granule cells (>9%) in the model used for the present study (Pun et al., 2012), suggesting that the number of cells in the model is above the theoretical threshold to cause seizures.

Summary

PTEN deletion from hippocampal dentate granule cells can provoke epileptogenesis in animal models. Further, PTEN mutations in humans, as well as mutations in other mTOR pathway genes, are linked to epilepsy. The present results provide anatomical evidence that mTOR pathway hyperactivation can alter axonal structure and connectivity, providing new insights into the mechanisms by which mutations in this gene pathway contribute to epileptogenesis.

Acknowledgements

This work was supported by the National Institute of Neurological Disorders and Stroke (SCD, Award Numbers R01NS065020 and R01NS062806; CLL, NRSA F32NS083239). The content is solely the responsibility of the authors and does not necessarily represent the official views of the National Institute of Neurological Disorders and Stroke or the National Institutes of Health. We would also like to thank Raymund Y. K. Pun for his work injecting dentate granule cells with biocytin and Keri Kaeding for help with manuscript preparation.

References

Acsády L, Kamondi A, Sík A, Freund T, Buzsáki G. GABAergic Cells Are the Major Postsynaptic Targets of Mossy Fibers in the Rat Hippocampus. The Journal of Neuroscience. 1998; 18:3386–3403. [PubMed: 9547246]

Ahn S, Joyner AL. Dynamic Changes in the Response of Cells to Positive Hedgehog Signaling during Mouse Limb Patterning. Cell. 2004; 118:505–516. [PubMed: 15315762]

Ahn S, Joyner AL. In vivo analysis of quiescent adult neural stem cells responding to Sonic hedgehog. Nature. 2005; 437:894–897. [PubMed: 16208373]

Amaral DG, Ishizuka N, Claiborne B. Neurons, numbers and the hippocampal network. Prog Brain Res. 1990; 83:1–11. [PubMed: 2203093]

Amaral DG, Scharfman HE, Lavenex P. The dentate gyrus: fundamental neuroanatomical organization (dentate gyrus for dummies). Prog Brain Res. 2007; 163:3–22. [PubMed: 17765709]

Amiri A, Cho W, Zhou J, Birnbaum SG, Sinton CM, McKay RM, Parada LF. Pten Deletion in Adult Hippocampal Neural Stem/Progenitor Cells Causes Cellular Abnormalities and Alters Neurogenesis. The Journal of Neuroscience. 2012; 32:5880–5890. [PubMed: 22539849]

Bateup HS, Takasaki KT, Saulnier JL, Denefrio CL, Sabatini BL. Loss of Tsc1 in vivo impairs hippocampal mGluR-LTD and increases excitatory synaptic function. J Neurosci. 2011; 31:8862–8869. [PubMed: 21677170]

Ben-Ari Y, Dudek FE. Primary and secondary mechanisms of epileptogenesis in the temporal lobe: there is a before and an after. Epilepsy currents / American Epilepsy Society. 2010; 10:118–125. [PubMed: 20944823]

Blaabjerg M, Zimmer J. The dentate mossy fibers: structural organization, development and plasticity. Prog Brain Res. 2007; 163:85–107. [PubMed: 17765713]

Borges K, Gearing M, McDermott DL, Smith AB, Almonte AG, Wainer BH, Dingledine R. Neuronal and glial pathological changes during epileptogenesis in the mouse pilocarpine model. Exp Neurol. 2003; 182:21–34. [PubMed: 12821374]

Brewster AL, Lugo JN, Patil VV, Lee WL, Qian Y, Vanegas F, Anderson AE. Rapamycin reverses status epilepticus-induced memory deficits and dendritic damage. PLoS One. 2013; 8:e57808. [PubMed: 23536771]

Buckmaster PS, Lew FH. Rapamycin Suppresses Mossy Fiber Sprouting But Not Seizure Frequency in a Mouse Model of Temporal Lobe Epilepsy. The Journal of Neuroscience. 2011; 31:2337–2347. [PubMed: 21307269]

Cameron MC, Zhan RZ, Nadler JV. Morphologic integration of hilar ectopic granule cells into dentate gyrus circuitry in the pilocarpine model of temporal lobe epilepsy. J Comp Neurol. 2011; 519:2175–2192. [PubMed: 21455997]

Choi YJ, Di Nardo A, Kramvis I, Meikle L, Kwiatkowski DJ, Sahin M, He X. Tuberous sclerosis complex proteins control axon formation. Genes Dev. 2008; 22:2485–2495. [PubMed: 18794346]

Claiborne BJ, Amaral DG, Cowan WM. A light and electron microscopic analysis of the mossy fibers of the rat dentate gyrus. J Comp Neurol. 1986; 246:435–458. [PubMed: 3700723]

Curia G, Longo D, Biagini G, Jones RSG, Avoli M. The pilocarpine model of temporal lobe epilepsy. Journal of Neuroscience Methods. 2008; 172:143–157. [PubMed: 18550176]

Danzer S, He X, Loepke A, McNamara J. Structural plasticity of dentate granule cell mossy fibers during the development of limbic epilepsy. Hippocampus. 2010; 20:113–124. [PubMed: 19294647]

Dudek, FE.; Sutula, TP. Epileptogenesis in the dentate gyrus: a critical perspective.. In: Helen, ES., editor. Progress in Brain Research. Vol. 163. Elsevier; 2007. p. 755-773.

Faulkner RL, Jang MH, Liu XB, Duan X, Sailor KA, Kim JY, Ge S, Jones EG, Ming GL, Song H, Cheng HJ. Development of hippocampal mossy fiber synaptic outputs by new neurons in the adult brain. Proc Natl Acad Sci U S A. 2008; 105:14157–14162. [PubMed: 18780780]

Frotscher M. Mossy fiber synapses on glutamate decarboxylase-immunoreactive neurons: evidence for feed-forward inhibition in the CA3 region of the hippocampus. Exp Brain Res. 1989; 75:441–445. [PubMed: 2721621]

Goussakov IV, Fink K, Elger CE, Beck H. Metaplasticity of mossy fiber synaptic transmission involves altered release probability. J Neurosci. 2000; 20:3434–3441. [PubMed: 10777806]

Haws ME, Jaramillo TC, Espinosa F, A JW, Stuber GD, Sparta DR, Tye KM, Russo SJ, Parada LF, Stavarache M, Kaplitt M, Bonci A, Powell CM. PTEN knockdown alters dendritic spine/protrusion morphology, not density. J Comp Neurol. 2014; 522:1171–1190. [PubMed: 24264880]

Henze DA, Wittner L, Buzsaki G. Single granule cells reliably discharge targets in the hippocampal CA3 network in vivo. Nat Neurosci. 2002; 5:790–795. [PubMed: 12118256]

Hester MS, Danzer SC. Accumulation of abnormal adult-generated hippocampal granule cells predicts seizure frequency and severity. J Neurosci. 2013; 33:8926–8936. [PubMed: 23699504]

Hester, MS.; Danzer, SC. Hippocampal granule cell pathology in epilepsy - A possible structural basis for comorbidities of epilepsy? Epilepsy & behavior. E&B; 2014.

Howell K, Hopkins N, McLoughlin P. Combined confocal microscopy and stereology: a highly efficient and unbiased approach to quantitative structural measurement in tissues. Exp Physiol. 2002; 87:747–756. [PubMed: 12530405]

Hsu, D. The dentate gyrus as a filter or gate: a look back and a look ahead.. In: Helen, ES., editor. Progress in Brain Research. Vol. 163. Elsevier; 2007. p. 601-613.

Huang X, Zhang H, Yang J, Wu J, McMahon J, Lin Y, Cao Z, Gruenthal M, Huang Y. Pharmacological inhibition of the mammalian target of rapamycin pathway suppresses acquired epilepsy. Neurobiol Dis. 2010; 40:193–199. [PubMed: 20566381]

Ishizuka N, Cowan WM, Amaral DG. A quantitative analysis of the dendritic organization of pyramidal cells in the rat hippocampus. J Comp Neurol. 1995; 362:17–45. [PubMed: 8576427]

Jones RS, Heinemann U. Synaptic and intrinsic responses of medical entorhinal cortical cells in normal and magnesium-free medium in vitro. J Neurophysiol. 1988; 59:1476–1496. [PubMed: 2898511]

Kim JY, Duan X, Liu CY, Jang MH, Guo JU, Pow-anpongkul N, Kang E, Song H, Ming GL. DISC1 regulates new neuron development in the adult brain via modulation of AKT-mTOR signaling through KIAA1212. Neuron. 2009; 63:761–773. [PubMed: 19778506]

Kwon CH, Luikart BW, Powell CM, Zhou J, Matheny SA, Zhang W, Li Y, Baker SJ, Parada LF. Pten regulates neuronal arborization and social interaction in mice. Neuron. 2006; 50:377–388. [PubMed: 16675393]

Kwon CH, Zhu X, Zhang J, Knoop LL, Tharp R, Smeyne RJ, Eberhart CG, Burger PC, Baker SJ. Pten regulates neuronal soma size: a mouse model of Lhermitte-Duclos disease. Nat Genet. 2001; 29:404–411. [PubMed: 11726927]

Lasarge CL, Danzer SC. Mechanisms regulating neuronal excitability and seizure development following mTOR pathway hyperactivation. Frontiers in molecular neuroscience. 2014; 7:18. [PubMed: 24672426]

Lorente De Nó R. Studies on the structure of the cerebral cortex. II. Continuation of the study of the ammonic system. Journal für Psychologie und Neurologie. 1934; 46:113–177.

Luikart BW, Schnell E, Washburn EK, Bensen AL, Tovar KR, Westbrook GL. Pten knockdown in vivo increases excitatory drive onto dentate granule cells. J Neurosci. 2011; 31:4345–4354. [PubMed: 21411674]

McAuliffe JJ, Bronson SL, Hester MS, Murphy BL, Dahlquist-Topala R, Richards DA, Danzer SC. Altered patterning of dentate granule cell mossy fiber inputs onto CA3 pyramidal cells in limbic epilepsy. Hippocampus. 2011; 21:93–107. [PubMed: 20014385]

Ming GL, Song H. Adult neurogenesis in the mammalian central nervous system. Annu Rev Neurosci. 2005; 28:223–250. [PubMed: 16022595]

Morgan RJ, Soltesz I. Nonrandom connectivity of the epileptic dentate gyrus predicts a major role for neuronal hubs in seizures. Proceedings of the National Academy of Sciences. 2008; 105:6179–6184.

Murphy BL, Hofacer RD, Faulkner CN, Loepke AW, Danzer SC. Abnormalities of granule cell dendritic structure are a prominent feature of the intrahippocampal kainic acid model of epilepsy despite reduced postinjury neurogenesis. Epilepsia. 2012; 53:908–921. [PubMed: 22533643]

Nakamura T, Colbert MC, Robbins J. Neural crest cells retain multipotential characteristics in the developing valves and label the cardiac conduction system. Circulation research. 2006; 98:1547–1554. [PubMed: 16709902]

Nek N, Schwegler H, Crusio WE, Frotscher M. Are the fine-structural characteristics of mouse hippocampal mossy fiber synapses determined by the density of mossy fiber axons? Neurosci Lett. 1993; 158:75–78. [PubMed: 8233075]

Parent, JM.; Kron, MM. Neurogenesis and Epilepsy.. In: Noebels, JL., et al., editors. Jasper's Basic Mechanisms of the Epilepsies. National Center for Biotechnology Information (US); Bethesda (MD): 2012.

Patel MN, McNamara JO. Selective enhancement of axonal branching of cultured dentate gyrus neurons by neurotrophic factors. Neuroscience. 1995; 69:763–770. [PubMed: 8596646]

Paxinos, G.; Franklin, KBJ. The Mouse Brain in Stereotaxic Coordinates. Academic Press; San Diego: 2001.

Pierce JP, Milner TA. Parallel increases in the synaptic and surface areas of mossy fiber terminals following seizure induction. Synapse (New York, NY). 2001; 39:249–256.

Pun RY, Rolle IJ, Lasarge CL, Hosford BE, Rosen JM, Uhl JD, Schmeltzer SN, Faulkner C, Bronson SL, Murphy BL, Richards DA, Holland KD, Danzer SC. Excessive activation of mTOR in

postnatally generated granule cells is sufficient to cause epilepsy. Neuron. 2012; 75:1022–1034. [PubMed: 22998871]

Rushton WAH. A theory of the effects of fibre size in medullated nerve. The Journal of Physiology. 1951; 115:101–122. [PubMed: 14889433]

Santos VR, de Castro OW, Pun RY, Hester MS, Murphy BL, Loepke AW, Garcia-Cairasco N, Danzer SC. Contributions of mature granule cells to structural plasticity in temporal lobe epilepsy. Neuroscience. 2011; 197:348–357. [PubMed: 21963349]

Scharfman HE, Pierce JP. New insights into the role of hilar ectopic granule cells in the dentate gyrus based on quantitative anatomic analysis and three-dimensional reconstruction. Epilepsia. 2012; 53(Suppl 1):109–115. [PubMed: 22612815]

Seress L, Abraham H, Paleszter M, Gallyas F. Granule cells are the main source of excitatory input to a subpopulation of GABAergic hippocampal neurons as revealed by electron microscopic double staining for zinc histochemistry and parvalbumin immunocytochemistry. Exp Brain Res. 2001; 136:456–462. [PubMed: 11291726]

Shibley H, Smith BN. Pilocarpine-induced status epilepticus results in mossy fiber sprouting and spontaneous seizures in C57BL/6 and CD-1 mice. Epilepsy Res. 2002; 49:109–120. [PubMed: 12049799]

Singh SP, He X, McNamara JO, Danzer SC. Morphological changes among hippocampal dentate granule cells exposed to early kindling-epileptogenesis. Hippocampus. 2013; 23:1309–1320. [PubMed: 23893783]

Sperow M, Berry RB, Bayazitov IT, Zhu G, Baker SJ, Zakharenko SS. Phosphatase and tensin homologue (PTEN) regulates synaptic plasticity independently of its effect on neuronal morphology and migration. The Journal of Physiology. 2012; 590:777–792. [PubMed: 22147265]

Sutula T, Zhang P, Lynch M, Sayin U, Golarai G, Rod R. Synaptic and axonal remodeling of mossy fibers in the hilus and supragranular region of the dentate gyrus in kainate-treated rats. J Comp Neurol. 1998; 390:578–594. [PubMed: 9450537]

Ting JT, Daigle TL, Chen Q, Feng G. Acute brain slice methods for adult and aging animals: application of targeted patch clamp analysis and optogenetics. Methods Mol Biol. 2014; 1183:221–242. [PubMed: 25023312]

Upreti C, Otero R, Partida C, Skinner F, Thakker R, Pacheco LF, Zhou ZY, Maglakelidze G, Veliskova J, Velisek L, Romanovicz D, Jones T, Stanton PK, Garrido-Sanabria ER. Altered neurotransmitter release, vesicle recycling and presynaptic structure in the pilocarpine model of temporal lobe epilepsy. Brain. 2012; 135:869–885. [PubMed: 22344585]

Wong M. A critical review of mTOR inhibitors and epilepsy: from basic science to clinical trials. Expert review of neurotherapeutics. 2013; 13:657–669. [PubMed: 23739003]

Yamawaki R, Thind K, Buckmaster PS. Blockade of excitatory synaptogenesis with proximal dendrites of dentate granule cells following rapamycin treatment in a mouse model of temporal lobe epilepsy. J Comp Neurol. 2015; 523:281–297. [PubMed: 25234294]

Zeng L-H, Rensing NR, Wong M. The Mammalian Target of Rapamycin Signaling Pathway Mediates Epileptogenesis in a Model of Temporal Lobe Epilepsy. The Journal of Neuroscience. 2009; 29:6964–6972. [PubMed: 19474323]

Zhao C, Deng W, Gage FH. Mechanisms and Functional Implications of Adult Neurogenesis. Cell. 2008; 132:645–660. [PubMed: 18295581]

Zhou J, Blundell J, Ogawa S, Kwon CH, Zhang W, Sinton C, Powell CM, Parada LF. Pharmacological inhibition of mTORC1 suppresses anatomical, cellular, and behavioral abnormalities in neural-specific Pten knock-out mice. J Neurosci. 2009; 29:1773–1783. [PubMed: 19211884]

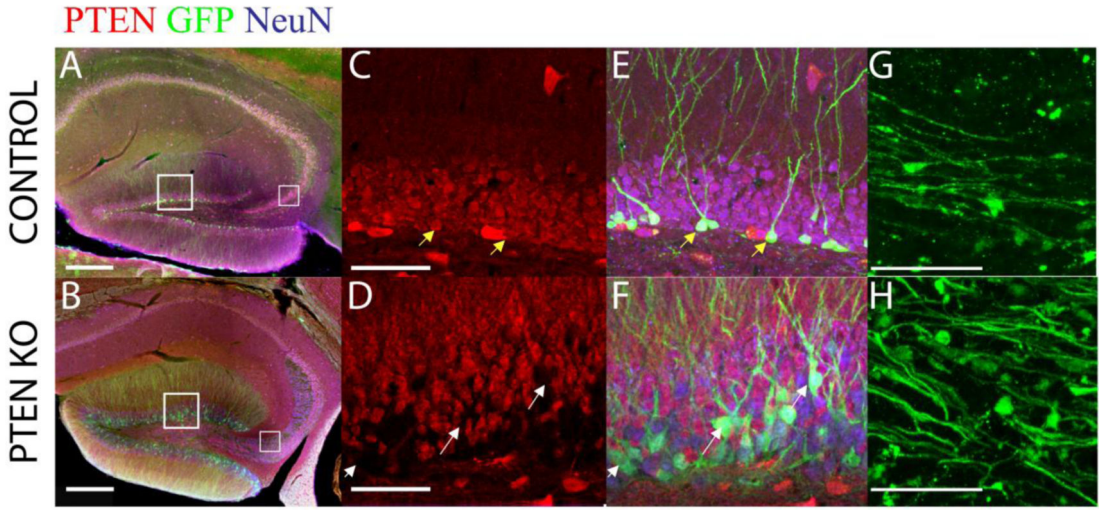

Figure 1. PTEN deletion from a subset of adult born granule cells

Confocal optical sections from control and PTEN KO mice were immunostained for NeuN (blue), PTEN (red), and GFP (green). **(A/B)** Hippocampi from control and PTEN KO mice have GFP-expressing cells in the dentate gyrus, with most GFP+ cells located near the hilar border. Of note, the thickening of the CA3 stratum lucidum is evident in the low power image. **(C-F)** Control dentate granule cells expressed PTEN (NeuN+/PTEN+; yellow arrows), whereas PTEN KO cells appear as gaps in PTEN staining (NeuN+/PTEN−; white arrows). **(G/H)** Mossy fiber axons of GFP-expressing cells were imaged in CA3. PTEN KO mice appear to have more axons in stratum lucidum. Scale bar = 200μm (A/B); 50μm (C-F); 20μm (G/H).

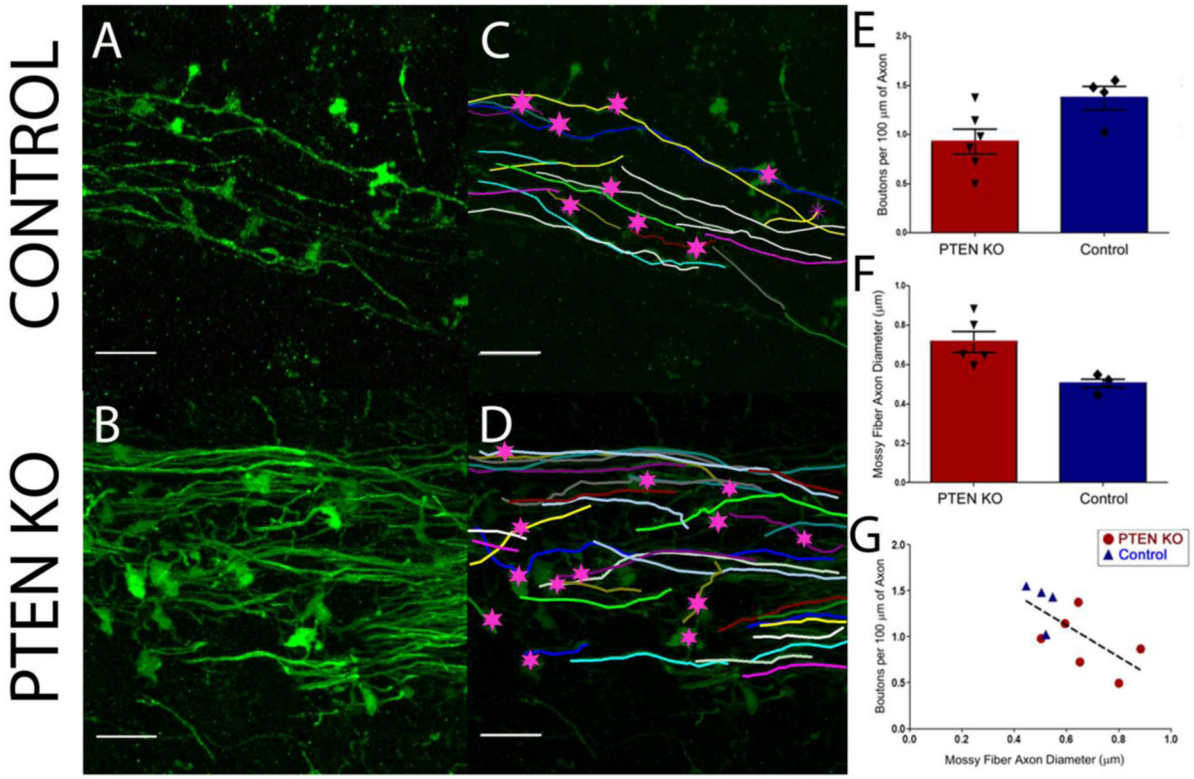

Figure 2. Structural changes of mossy fiber axons in PTEN-knockout mice

(A/B) Stratum lucidum in CA3b of control and PTEN KO mice showing GFP labeled mossy fiber axons. **(C/D)** Neurolucida reconstructions of the GFP-labeled axons shown in A and B. The number of mossy fiber bouton per 100 µm axon was decreased (E) while axon diameter (F) was increased in PTEN-knockout mice compared to controls ($p<0.05$, t-test). G: Mossy fiber axon diameter was correlated with boutons per 100 µm of axon length, in which thicker axons had a lower bouton density ($R=0.680$, $p=0.030$, Pearson Correlation). Scale bar = 10µm.

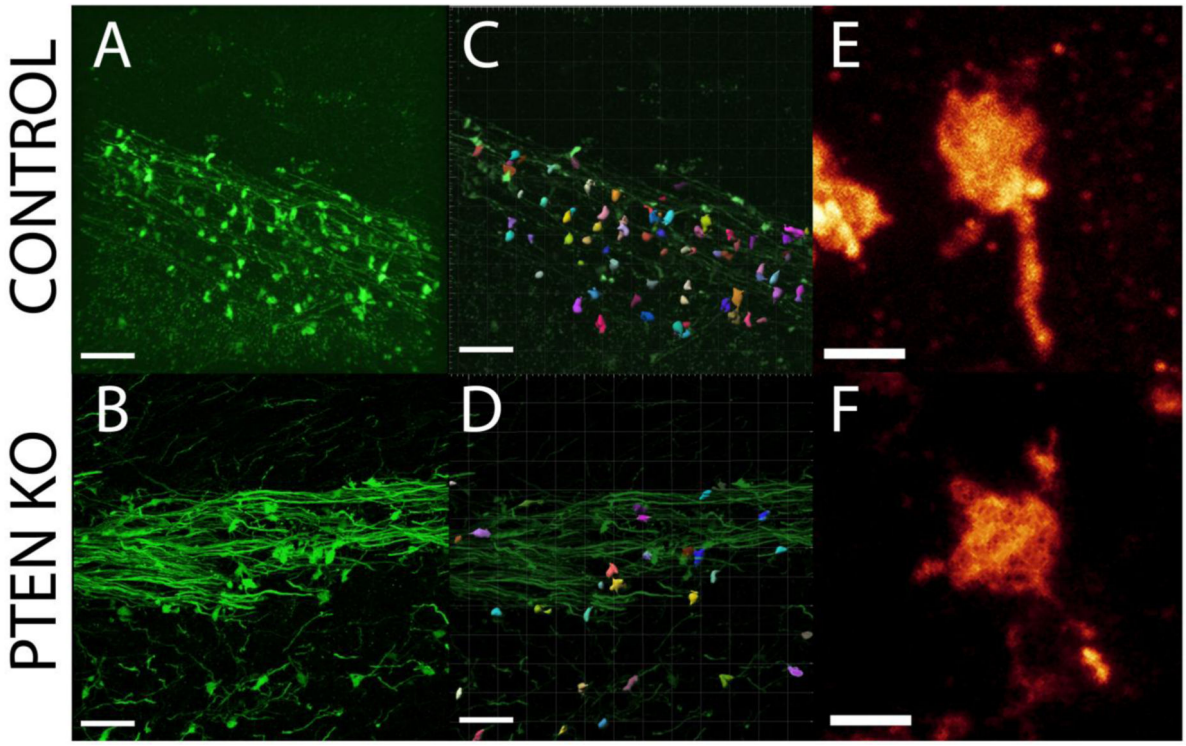

Figure 3. Mossy fiber bouton structure

(A/B) Confocal images of GFP-expressing axons in stratum lucidum of CA3b in control and PTEN KO mice. **(C/D)** Surface models of boutons created from control and PTEN KO mice using Imaris software. No differences in bouton volume were detected between controls and PTEN-knockout mice. **(E/F)** High resolution confocal images showing mossy fiber boutons from control and PTEN KO mice. Scale bar = 20 μm (A-D); 2 μm (E/F).

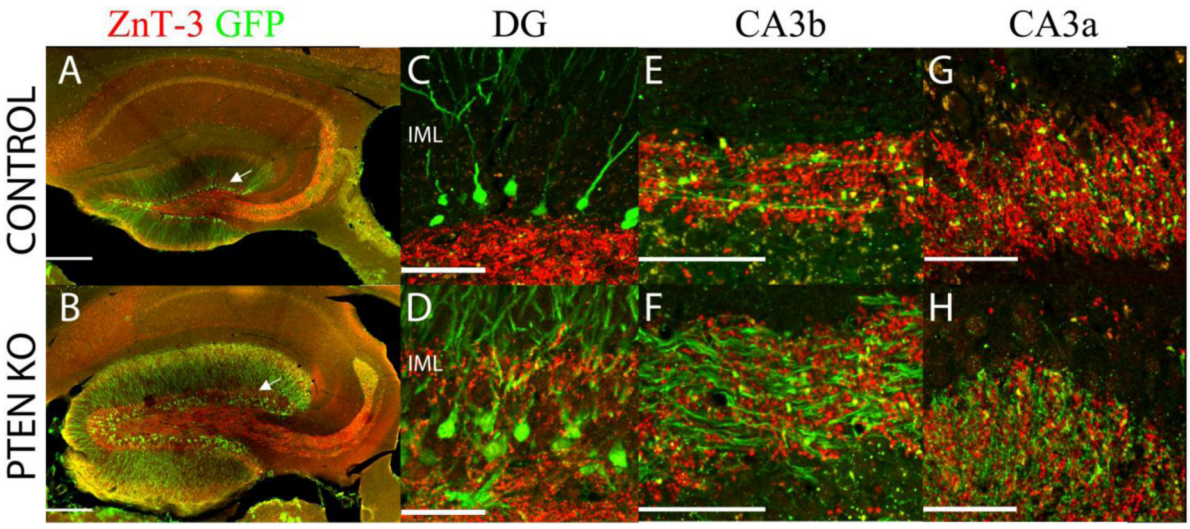

Figure 4. Mossy fiber terminals

Hippocampi from control and PTEN KO mice were immunostained for GFP (green) and ZnT-3 (red), which labels zinc rich mossy fiber terminals. **(A/B)** Low power images of merged ZnT3 and GFP. The control section exhibits the normal mossy fiber axon terminal field, while mossy fiber labeling is evident in the dentate inner molecular layer (IML; arrow) in the PTEN KO mice. **(C/D)** Robust ZnT-3 labeling is present in the IML of the PTEN KO animal, but is absent from control tissue. Confocal images from CA3b **(E/F)** and CA3a **(G/H)** reveal mossy fiber terminals located at high density throughout the stratum lucidum of control and PTEN KO mice, even though inter-bouton interval is greater along the axons of PTEN KO mice. Scale bar = 200μm (A/B); 50μm (C-H).

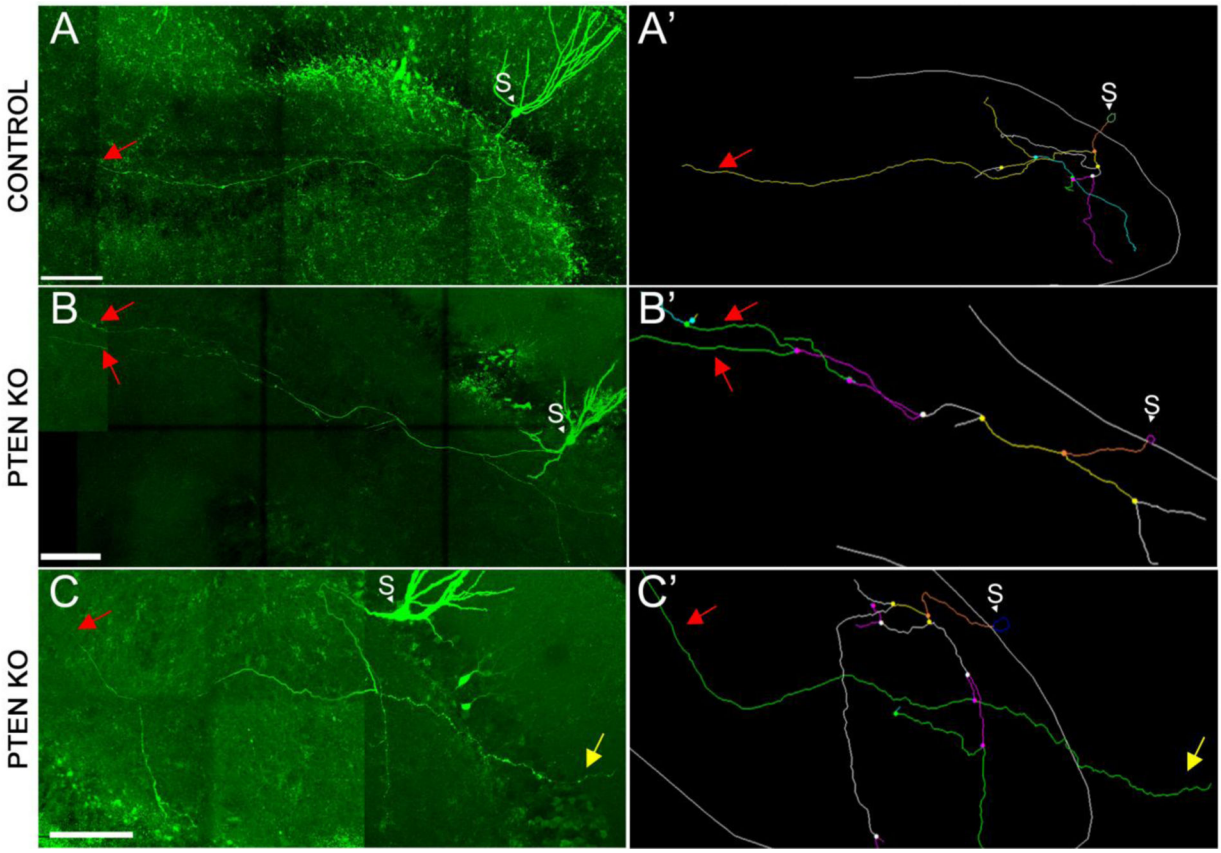

Figure 5. Mossy fiber axons of PTEN KO mice exhibit abnormal growth

(A-C) Confocal images of biocytin-filled granule cells from control and PTEN KO mice. Right panels show reconstructions generated using Neurolucida software. Control cells (A) collaterized extensively in the hilus, but project only a single fiber into CA3. PTEN KO cells exhibit irregular mossy fiber growth, with some cells extending multiple axon fibers into CA3 (B and B') or sprouting into the dentate molecular layer (C and C'). Red arrows highlight the axons that extended into CA3. Yellow arrows highlight the axon that extended into the dentate molecular layer. Scale bar = 100 μm.

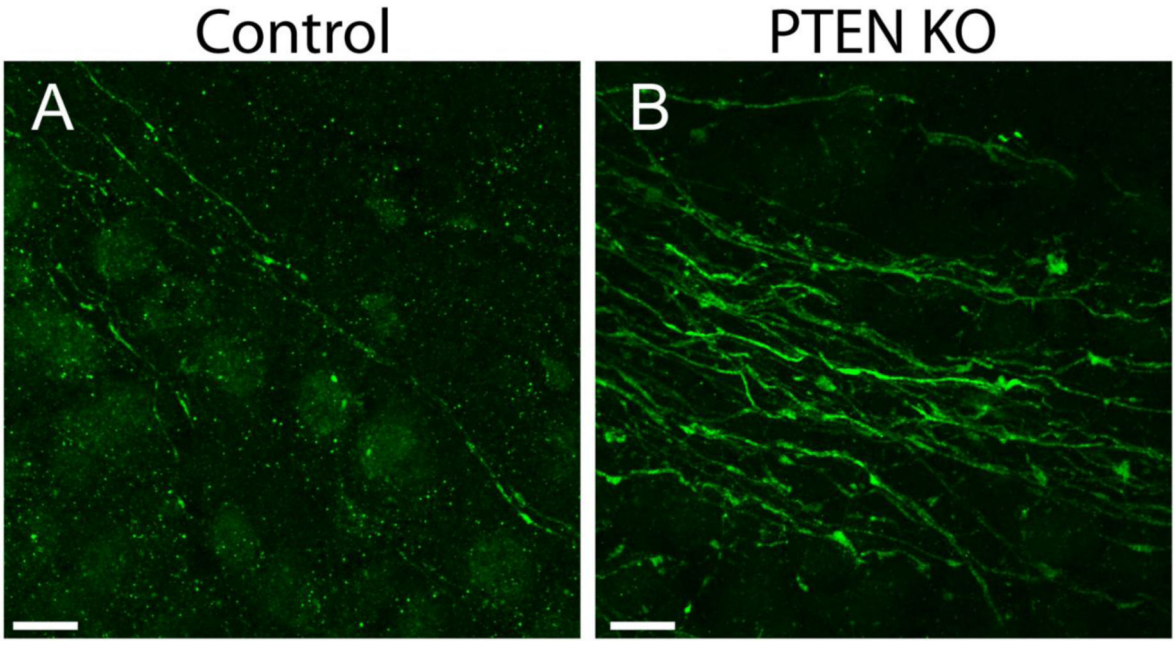

Figure 6. Morphological abnormalities in developing mossy fiber axons of PTEN KO cells

Confocal images of GFP-expressing mossy fiber axons in stratum lucidum of CA3b from control (A) and PTEN KO (B) mice four weeks after gene deletion illustrate the early onset of axonal hypertrophy. Scale bar = 10 μm.